First principles calculations of ZnS:Te energy levels

Jingbo Li and Lin-Wang Wang
Lawrence Berkeley National Laboratory, Berkeley, California 94720
(Received 7 January 2003; published 27 May 2003)

A comprehensive density-functional calculation for the ZnS:Te isoelectronic impurity state is presented. We deploy a charge patching method that enables us to calculate systems containing thousands of atoms. We found that the impurity state is only weakly localized, and previous calculations using 64-atom cells were severely unconverged. Our calculated impurity binding energy agrees with experimental photoluminescence excitation spectrum. We have analyzed the impurity wave function in both real space and the reciprocal space, and in terms of the host bulk valence bands. We have also calculated the Stokes shifts and Jahn-Teller effects. We found small Stokes shift compared to the experimental results, which might indicate the limitations of the current method. We also calculated the Te_n clusters and their impurity states. We found six (counting spin) bound states inside the band gap of ZnS for all $1 \leqslant n \leqslant 4$. We obtained pressure coefficients for Te_n, all close to the value of bulk ZnS. This is consistent with the fact that the impurity states of Te_n consist almost entirely of the bulk valence bands of ZnS. Finally, we have calculated the effects of spin-orbit coupling for the impurity state eigenenergies.

DOI: 10.1103/PhysRevB.67.205319 PACS number(s): 71.15.−m, 71.55.−i, 78.66.Hf

I. INTRODUCTION

The concept of isoelectronic trap states for semiconductor alloys was originally introduced in the 1960's.[1,2] Although the isoelectronic impurity has the same number of valence electrons as the host atom it replaces, it can induce a bound localized state if its atomic size and electronegativity are sufficiently different from its host atom. This often happens in III-V compounds, e.g., the As and P substitutions in GaN (denoted as GaN:As and GaN:P, respectively), as well as II-VI compounds: CdS:Te and ZnS:Te. In recent years, there is a renewed interest in these isoelectronic trap states. This is partly due to the realization that the alloy counterparts of these isoelectronic trap systems (e.g., $GaAs_xN_{1-x}$ from GaN:As and GaAs:N, In_xGa_{1-x} N from GaN:In) constitute a new class of ''unconventional'' alloys, with their electronic structures unlike the conventional crystal bulk band structures.[3–12] The recent successful applications of these ''unconventional'' alloys in blue lasers and solar cells have added urgencies for the understanding of these systems.

To understand the alloy systems, one first needs to understand its impurity limit: the isoelectronic trap state. Despite the fact that this is an old topic, the nature of the isoelectronic trap state is still not well understood. This is especially true for valence-band-induced isoelectronic trap states, such as, GaN:As, GaN:P, CdS:Te, and ZnS:Te. These systems have impurity levels slightly above the top of the valence band. In the experimental spectroscopy measurement, broad peaks are observed for these valence-band-induced isoelectronic trap states, in contrast to conduction-band-induced isoelectronic trap states (e.g., GaAs:N) where sharp peaks are often observed. As a result, even the exact impurity energies are not known for the valence-band-induced isoelectronic trap states. The broad peaks themselves are indications of large electron-phonon couplings. But the very nature of this strong coupling is not clear, especially given the fact that these impurity levels are usually only weakly bound and not strongly localized.[12,13]

Theoretically, this is also a challenging problem. Early theoretical work has focused on the cause of the bound trap state. Hopfield *et al.*[14] have attributed the cause to the difference in electronegativities between the isoelectronic impurity atom and the host atom. Allen,[15] on the other hand, considered the effect of lattice deformation due to different sizes of impurity atoms. This causes a strain field effect, which is related to the bulk deformation potential of the host. Phillips[16] further argued that the electron polarization and screening can also play an important role, which can significantly reduce the binding energy. However, to get quantitatively accurate results, numerical calculations are needed. Green's-function methods[17] and tight-binding methods[18] have been used to calculate the impurity levels. But they are highly parametrized. Recently, empirical pseudopotential methods (EPM) have been used to study this problem.[5] However, there are some uncertainties in these EPM calculations since only the binary systems are fitted in EPM. A more reliable way is to use the *ab initio* density-functional theory (DFT). The problem here is the size of the system attainable by DFT. Recent DFT calculations on the isoelectronic trap state used 64-atom unit cells.[19,20] In a previous work,[13] we pointed out that the 64-atom cells are severely unconverged, strong impurity-impurity coupling exists, and, as a result, the binding energies of the impurity states are severely overestimated. Recently, we have developed a charge patching method that allows thousand atom *ab initio* calculations. This makes it possible to reinvestigate the isoelectronic impurity problem via *ab initio* calculations.

In this work, we will choose one well-studied valence-band-induced isoelectronic trap state system: ZnS:Te. The purpose here is to conduct a detailed study of this system using the *ab initio* charge patching method. Not only can this shed light on the physical properties of this important system (e.g., the energy level, localization, clusters, electron-phonon interactions), it can also be used to test the applicability of the DFT method to such isoelectronic impurity problems. $ZnS_{1-x}Te_x$ is a technologically important material. Besides

being lattice matched to GaAs and Si substrates, its wide band gap (2.26 eV~3.6 eV) (Ref. 21) makes it a promising candidate for blue and green LED and lasers. Recently, experiments[21,22] have found that the radiative recombination rate of ZnS_xTe_{1-x} films is significantly higher than the ZnS and ZnSe thin films. This further improves its applicability in optoelectronic devices.

The spectroscopies of ZnS:Te have been studied by many experimental groups.[23–29] When a small amount of Te is introduced into ZnS, one finds the following main phenomena.

(1) *Bound excitons for single impurity Te and Te_n clusters.* Fuskushima and Shionoya[24] identified the emission and excitation peaks for single impurity Te in cubic ZnS as 3.14 eV and 3.7 eV, respectively. They estimated the zero-phonon line at 3.4 eV. Mind that, the intrinsic *A* exciton absorption line of bulk ZnS is at 3.79 eV. This indicates a bound impurity level above the top of the valence band. As the composition of Te increases, one can observe the photoemission of excitons related to Te_n clusters.[24,28–32] The corresponding impurity binding energies increase as Te forms larger clusters. As mentioned before, unlike the conduction-band-induced isoelectronic levels, the emission peaks in ZnS:Te impurity and Te_n clusters are typically broad, with line width of a few tenths of eV.

(2) *Anomalously large pressure coefficient of single impurity exciton energy.* The pressure dependence of photoluminescence (PL) and absorption spectra are powerful tools to study the nature of impurity states. For shallow impurity systems, e.g., GaAs:Si, their impurity states mainly consist of the wave functions of host bulk state. Thus the pressure coefficient of the impurity level is almost the same as that of the host crystal. In GaAs:N, the pressure coefficient of the nitrogen level is 40 meV/GPa, which is much smaller than that of bulk GaAs (which is 110 meV/GPa). This can be explained[33] by the Γ_{1c}, X_{1c}, and L_{1c} components in the impurity wave function, which have different signs of pressure coefficient, thus cancel each other out. Recently Fang and Li[32] have observed a higher pressure coefficient of Te_1 (single Te impurity) in ZnS_xTe_{1-x} (89 meV/GPa), compared to the bulk ZnS (which has a pressure coefficient of 63 meV/GPa). However, for the Te_n ($n \geqslant 2$) clusters, their pressure coefficients are similar to that of bulk ZnS.[31] It is not clear what causes the large pressure coefficient for Te_1. It is not even sure whether that is only an anomaly in the measured samples.

(3) *Large Stokes shift in ZnS:Te.* Stokes shift is defined as the energy difference between the absorption spectrum and PL spectrum. Closely related to the broad peaks in the spectra, the Stokes shift of ZnS:Te is large, about 0.56 eV.[24] As discussed before, this is an indication of large electron-phonon coupling. A simple way to describe this coupling is to use the Franck-Condon picture. It is interesting to know what kind of atomic relaxation exists in the excited state, and whether a simple DFT method can be used to predict such relaxations.

In this paper, we will use the local-density approximation (LDA) of DFT to study ZnS:Te. We like to address the following questions: (1) Can LDA produce a localized state in ZnS:Te? If so, how large is the impurity binding energy? (2) How different is the final converged result compared to the previous unconverged 64-atom result? (3) How good is the calculated impurity energy level compared to the experimental result? Actually, which experimental results [photoluminescence, zero-phonon line (ZPL), or photoluminescence excitation (PLE)] should we compare to? (4) Can we get large Stokes shift using Franck-Condon picture by LDA calculation? (5) Does strong Jahn-Teller distortion exist in the optically excited ZnS:Te system? (6) What are the calculated energy levels of Te_n clusters and their pressure coefficients? How do they compare to the experimental results? (7) Last, because spin-orbit splittings in ZnS and ZnTe are rather different, what is the role of spin-orbit splitting in ZnS:Te?

The remainder of the paper is organized as follows: In Sec. II we explain the calculation method, in Sec. III, we discuss our results, and in Sec. IV, conclusions are provided.

II. CALCULATION METHOD

A. LDA calculations and atomic relaxation

In this study we have used a self-consistent plane-wave pseudopotential method (PWP), based on local-density approximation of the density-function theory. We have used the Perdew and Zunger parametrization for the LDA exchange-correlation function.[34] The single-particle wave function ψ_i and its eigenenergy ϵ_i are solved via Schrödinger's (Kohn-Sham) equation,

$$\left[-\frac{1}{2}\nabla^2 + V(\mathbf{r}) + \hat{\mathbf{V}}_{nonloc}\right]\psi_i = \boldsymbol{\epsilon_i}\boldsymbol{\psi_i}, \tag{1}$$

where the local potential $V(\mathbf{r})$ is calculated from the occupied charge density $\rho(r)$ via the LDA formula, and $\hat{V}_{nonloc}$ is the nonlocal part of the pseudopotential. We have used norm conserving pseudopotentials. For the Zn atom we have included the *d* electron in its valence electrons, while for Te we have used a nonlinear core correction term for the exchange and correlation function.[35] A plane-wave kinetic energy cutoff of 50.0 Ry is used.[36]

Although there is a band-gap error in a typical LDA calculation, it is widely believed that this error only affects the conduction band. For valence band related properties, such as the band offsets, it has been shown that LDA produces good results.[37] Here, our impurity state is valence-band-induced, thus we can use the LDA to calculate its energy levels without further corrections.

When an impurity atom is placed in a 64-atom supercell, we have used the LDA total energy calculation to relax its atom positions. However, we have also tested a valence force field (VFF) model.[38] The use of this model can considerably speed up the calculation, and the test of this model is important since many previous calculations on similar systems have been carried out using similar VFF models. Our VFF model includes bond stretching and bond bending terms, with their strength parameters derived from LDA bulk calculations.

B. Charge patching method for large supercells

The impurity state in ZnS:Te is only weakly localized. As a result, to accurately calculate this state, a large supercell containing thousands of atoms is needed. In this paper, we will use a charge patching method (CPM) to carry out LDA calculations for large systems up to 4096 atoms.[39] In the CPM procedure, we first calculate a 64-atom periodic supercell $Zn_{32}S_{31}Te_1$, in a $2a\times2a\times2a$ cubic box, where a is the ZnS lattice constant (in this study, we have used $a=5.41$ Å, the experimental lattice constant). We place the Te atom at the center of this cubic box. We then fix the S atoms of the surface of this cubic box at their ideal face-center-cubic (fcc) positions, while relax the positions of all other atoms using either a full LDA total-energy calculation or a VFF calculation. A $2\times2\times2k$-point grid is used for this 64-atom supercell. A $80\times80\times80$ real space grid for the charge density is used. Meanwhile, a $a\times a\times a$ eight-atom cubic cell for bulk ZnS is calculated, and its charge density is stored in a $40\times40\times40$ real space grid. To generate the charge density for a large supercell with one Te atom at the center, a same dense real space grid is used (e.g., $320\times320\times320$ for the $8a$ cubic box). The charge density at the center $2a\times2a\times2a$ cubic box is taken from the above 64-atom calculation, and the rest of the charge density in the surrounding area is taken from the bulk ZnS calculation. On the single grid point layer between these two regions, average charge densities between the 64-atom cell results and the bulk ZnS results are used. Following the above procedure, the LDA charge density $\rho(r)$ of a large system is generated, without doing a self-consistent calculation. In our previous work,[39] it was shown that the above generated charge density is very close to the true LDA charge density via a full self-consistent calculation. The eigenenergy error produced by this method is in the range of 30 meV. After $\rho(r)$ is obtained, we can generate $V(\mathbf{r})$ easily using the LDA formula. Then the impurity state can be solved from Eq. (1) using a linear scaling folded spectrum method.[40] In this work, we will study three large systems: $Zn_{256}S_{255}Te_1$, $Zn_{864}S_{863}Te_1$, and $Zn_{2048}S_{2047}Te_1$. They correspond to periodic cubic boxes of sizes $4a$, $6a$, and $8a$, respectively. Note that, our largest 4096-atom system has 36 864 occupied states. It is far beyond the capability of the conventional LDA method even with the powerful supercomputers of nowadays. All our calculations are carried out on parallel supercomputers at National Energy Research Scientific Computing Center (NERSC).

C. Franck-Condon picture and Jahn-Teller distortion

ZnS and ZnTe are polar semiconductors, thus strong Fröhlich electron-phonon interactions for LO phonon modes exist. Experimental data[23–25] show that there is a large Stokes shift of ZnS:Te ($\sim$0.56 eV). One possible way to understand this Stokes shift is via the Franck-Condon picture.

The Franck-Condon picture is shown in Fig. 1(a). The photoabsorption and emission processes are assumed to be much faster than the atomic relaxations, thus during the process of the PLE (PL), the atomic structures before and after the absorption (emission) are assumed to be the same. Figure 1(b) shows the schematics of the impurity level. In this study

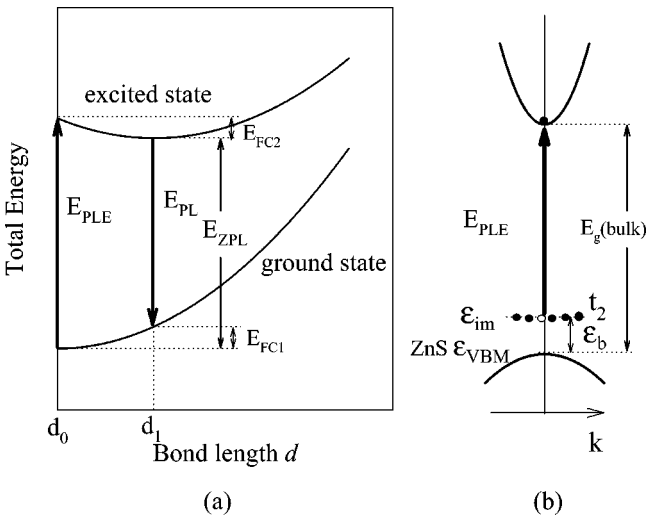

FIG. 1. (a) A configuration coordinate diagram for the Franck-Condon picture. We use the bond length d of Te and its nearest-neighbor Zn atom as the indicator of the general configuration coordinate (the full atomic configuration). (b) A schematic diagram for the impurity levels (ε_{im}) and their positions in the band gap of ZnS. ε_b is defined as the impurity binding energy. ϵ_{VBM} is the valence-band maximum energy of bulk ZnS.

we will define a single-particle impurity binding energy ε_b as $\varepsilon_{im}-\varepsilon_{VBM}$ [Fig. 1(b)]. Here, ε_{im} is the impurity eigenenergy from Eq. (1), ε_{VBM} is the bulk ZnS valence-band maximum (VBM) energy.[41] From Fig. 1, under the Franck-Condon picture, we see that $E_g-\epsilon_b$ should be identified with the PLE, not with PL, or ZPL. Given the large difference between PLE, PL and ZPL, this identification is important.

According to the Franck-Condon picture, the Stokes shift E_{Stokes} can be calculated as

$$E_{Stokes}=E_{PLE}-E_{PL}=E_{FC1}+E_{FC2}, \tag{2}$$

where E_{FC1} and E_{FC2} are two Franck-Condon relaxation energies:

$$E_{FC1}=E_{ZPL}-E_{PL} \tag{3}$$

for the ground state and

$$E_{FC2}=E_{PLE}-E_{ZPL} \tag{4}$$

for the excited state. To calculate $E_{FC1,2}$, we need to calculate the relaxation of the atomic structure in the excited state. We will use a constraint LDA approach to describe the excited state. In this approach, one top of valence-band state is unoccupied, and one bottom of conduction-band state is occupied [shown in Fig. 1(b)], and the total energy is calculated using the usual LDA formula. We will use 64-atom unit cells to study the Franck-Condon relaxation. We use the bond length d on the Te atom (shown in Fig. 2) as an indicator of the general Franck-Condon coordinate Q. In the calculation, for both the ground state and the excited state, we choose a d value (hence fix the four nearest-neighbor Zn atoms of Te), and then relax all the other atoms in the system, then obtain a LDA total energy corresponding to d. As a result, we will obtain the $E(d)$ curves for both the ground state and the

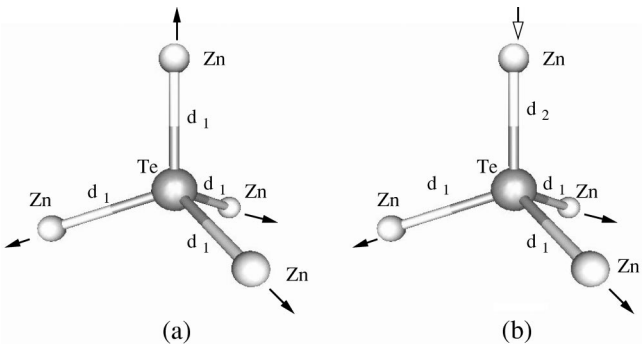

FIG. 2. One substitutional Te impurity (at the center). The four nearest Zn atoms can relax in two ways: (a) relax without changing the site T_d symmetry; (b) one bond length d_2 is different from other three bond lengths d_1, results in a trigonal C_{3v} symmetry. This relaxation corresponds to a Jahn-Teller distortion for an excited state.

excited state. They can be directly used in the Franck-Condon picture shown in Fig. 1.

Note that, our ground-state impurity level shown in Fig. 1(b) has a t_2 symmetry, and is thus threefold degenerated. This means that in an excited state when one of the six occupied electrons is missing from the impurity state, it is possible to lower the total energy by lowering the symmetry of the system, thus produce Jahn-Teller (JT) distortion. Recent experiments[42–44] suggested that the C_{3v} Jahn-Teller distortion is a common feature in deep impurity states, e.g., P and As impurities in ZnSe,[42] *n*-type doping Ga and Cl impurities in ZnSe,[43] and isolated Zn vacancy in ZnSe.[44] However, LDA calculations have failed to predict the experimentally observed JT effect in nitrogen impurities of ZnSe (Ref. 45) and in GaN:As and GaN:P impurities.[19] Here, we would like to see whether LDA calculation can produce a JT effect in our system. To do that, we keep the lengths of three bonds of Te as d_1 and one bond as d_2, as shown in Fig. 2(b). Then we independently change d_1 and d_2, obtain a two-dimensional energy function $E(d_1,d_2)$. JT effect will be found if the minimum energy of $E(d_1,d_2)$ corresponds to $d_1 \neq d_2$.

D. Spin-orbit interaction in the calculation

So far, in the above description of the LDA calculation, we have not included spin-orbit interaction. When all the valence states are occupied, it is believed that the spin-orbit splitting at the top of the valence band has very little effects on the total energies and atomic relaxations. However, the spin-orbit interaction does change the band structure, especially near the top of the valence band. The spin-orbit splitting for bulk ZnTe is extremely large, close to 0.97 eV, while the spin-orbit splitting for bulk ZnS is only about 0.07 eV. We will like to know what is the spin-orbit splitting in the ZnS:Te impurity state. In the folded spectrum method calculation of the impurity energy levels, we have added the spin-orbit interaction terms in Eq. (1). To do that, nonlocal pseudopotentials with relativistic effects of the core (which is the source of the strong spin-orbit interaction in the system) are used. In that case, wave function ψ_i in Eq. (1) is a spinor, with spin-up and spin-down components. Each component is described by an expansion of the plane-wave basis functions.

TABLE I. The structural properties of zinc-blende ZnS calculated in this work compared with PWP (Ref. 46), LAPW (Ref. 46), and experiment Ref. (48, 49). The calculated values for the lattice constant a_0, bulk modulus B_0, pressure derivative of the bulk modulus B', are obtained with a fit to the Murnaghan equation of state.

	Present cal.	PWP [a]	LAPW [a]	Experiment
a_0 (Å)	5.351	5.349	5.353	5.41 [b]
B_0 (GPa)	78.8	82	87	76.9 [b]
B'	4.4	4.6	4.9	4.91 [b]
dE_g/dp (meV/GPa)	62.3			63.5 [c]

[a]See Ref. 46.
[b]See Ref. 48.
[c]See Ref. 49.

III. RESULTS AND DISCUSSION

A. Bulk calculations

We have first checked our bulk calculations for ZnS and ZnTe, and compared our present results with previous LDA calculations using PWP,[46] the all-electron linearized-augmented plane-wave (LAPW) method,[46,47] and experiment.[48–50] The structural properties of bulk ZnS are listed in Table I. The eigenenergies of bulk ZnS and ZnTe at different special *k* points are listed in Tables II and III, respectively. From these three tables one can conclude that our current calculations are in excellent agreement with other LDA calculations and are also in good agreement with the experimental data, except for the well-known discrepancy in the band gap. But as we discussed before, since the impurity

TABLE II. The electronic eigenenergies (eV) of cubic ZnS ($a = 5.41$ Å) calculated in this work compared with other LDA calculations and experiment.

	Present cal.	PWP [a]	LAPW [a]	Experiment [b]
Γ_{1v}	−13.09	−13.07	−13.11	−13.5
Γ_{15v}	0	0	0	0
Γ_{1c}	1.818	1.839	1.814	3.80
Γ_{15c}	6.144	6.15	6.19	8.35
X_{1v}	−11.79	−11.77	−11.84	−12.0
X_{3v}	−4.73	−4.74	−4.70	−5.5
X_{5v}	−2.29	−2.29	−2.25	−2.5
X_{1c}	3.21	3.19	3.18	
X_{3c}	3.87	3.87	3.87	4.9
L_{1v}	−12.11	−12.10	−12.16	−12.4
L_{1v}	−5.44	−5.43	−5.38	−5.5
L_{3v}	−0.90	−0.90	−0.88	−1.4
L_{1c}	3.04	3.05	3.05	
L_{3c}	6.77	6.75	6.76	

[a]See Ref. 46.
[b]See Ref. 48.

TABLE III. The electronic eigen energies (eV) of cubic ZnTe ($a=6.089$ Å) calculated in this work compared with other LDA calculations and experiment.

	Present cal.	LAPW [a]	Experiment
Γ_{1v}	−11.931	−11.93	−13.0 [b]
Γ_{15v}	0	0	0 [b]
Γ_{1c}	0.78	0.96	2.39 [b]
Γ_{15c}	4.32	4.23	4.82 [c]
X_{1v}	−10.72	−10.72	−11.6 [b]
X_{3v}	−5.13	−5.18	−5.5 [b]
X_{5v}	−2.24	−2.25	−2.4 [b]
X_{1c}	2.15	2.13	3.05 [c]
X_{3c}	2.19	2.05	
L_{1v}	−11.041	−11.04	−12.0 [b]
L_{1v}	−5.30	−5.33	
L_{3v}	−0.933	−0.94	−1.1 [b]

[a]See Ref. 47.
[b]See Ref. 48.
[c]See Ref. 50.

state studied in this work is induced from the valence band, we do not expect that this band-gap error will cause any problem in our results.

B. Localized impurity state in ZnS:Te

Wave-function localization. The impurity potential has a tetrahedral symmetry. According to the irreducible representation of the T_d group, there could be three types of impurity states: a singlet state with a_1 symmetry, a doublet state with e symmetry, and a triplet state with t_2 symmetry. In the case of GaAs:N, there is a localized nitrogen state a_1(N) above the conduction-band minimum (CBM). In the present case of ZnS:Te, we found that the localized impurity states are threefold degenerated slightly above the VBM and they have t_2 symmetry. Figure 3 shows the sum of the wave-function squares of these three degenerated states for (a) 64-atom, (b) 512-atom, (c) 1728-atom, and (d) 4096-atom supercells. The

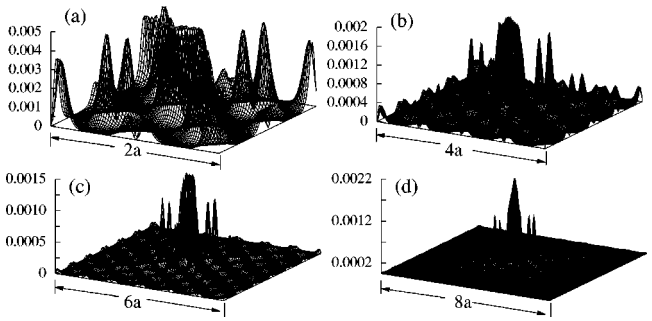

FIG. 3. Wave-function charge density of the impurity states of ZnS:Te on (001) cross sections. The charge-density sums of the three (not counting spin) degenerated impurity states are plotted: (a) for the 64-atom supercell; (b) for the 512-atom supercell; (c) for the 1728-atom supercell; and (d) for the 4096-atom supercell. a is the ZnS lattice constant. The x and y axes lie in the [100] and [010] directions. The unit of z axis is 0.333 e/Bohr^3.

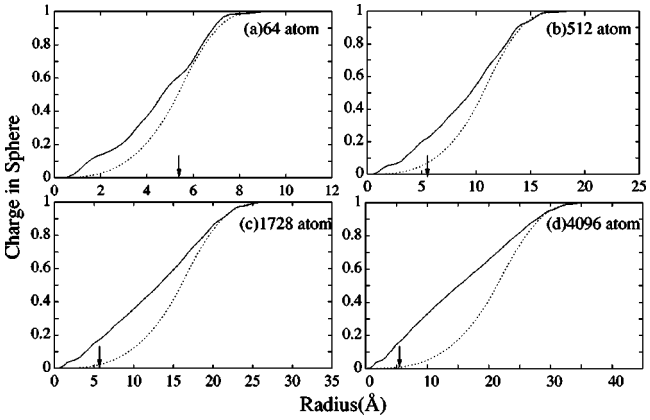

FIG. 4. The charge accumulation function $Q_i(R)$ of the impurity states for (a) 64-atom, (b) 512-atom, (c) 1728-atom, and (d) 4096-atom systems. Q_i is the charge inside a sphere of radius R. The arrows indicate the boundaries of 64-atom cells. The dashed lines are the results for uniform charge distributions.

impurity Te atom is placed at the center of the cell box. In the 64-atom cell some strong peaks exist near the surface S atom. There is no indication of a bound state in this 64-atom cell calculation. However, in the 4096-atom large supercell, the Te impurity state is clearly localized. The bound states have long-range tails in the (110) direction. Similar long-range tails were also found in GaAs:N for the $a_1(N)$ state.[39] To see the properties of localization more quantitatively, we have calculated the ''charge accumulation'' function $Q_i(R)$, which is the total charge of the wave function ψ_i inside a sphere of radius R centered at the impurity atom. The charge-density integration is done only within one supercell (with the impurity at its center), so when the spherical radius R is large enough to enclose the whole supercell, $Q_i(R)$ equals 1. Figure 4 shows the charge accumulation function of impurity state for (a) 64-atom, (b) 512-atom, (c) 1728-atom, and (d) 4096-atom supercell calculations. The results for uniform charge are also plotted as dotted curves for comparison. At a given radius $R_c=5.41$ Å indicated by vertical arrows in Fig. 4 (which corresponds to a sphere that touches the 64-atom cell boundary), the $Q_i(R)$ are 61.3%, 21.7%, 16.4%, and 15.9% for (a) 64-atom, (b) 512-atom, (c) 1728-atom, and (d) 4096-atom supercells respectively. Thus the charge distribution for the small supercell (64-atom) and large supercells is quite different. When the size of the supercell is larger than 512 atom, more than 80.0% of the wave function is outside R_c. This means the 64-atom cell is not large enough to describe the impurity localized state. For $R=2a$ and $3a$, $Q_i(R)$ for the 1728-atom (4096-atom) cell are 0.39 (0.37) and 0.68 (0.53), respectively. We see that there is a significant difference between the 1728-atom results and the 4096-atom results for large R, indicating that even the 1728-atom cell is not completely converged. This is confirmed by Fig. 3(c), where one can see the non-zero tail of the wave function extended to the supercell boundary. The unconvergence can also be demonstrated in the impurity binding energy.

Binding energies of the impurity states. The LDA band gap of ZnS in our calculation is much smaller than the ex-

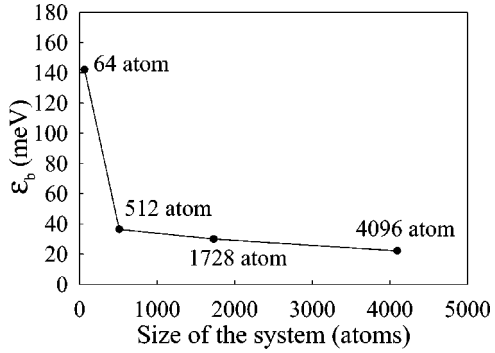

FIG. 5. Binding energy ε_b of ZnS:Te as a function of the size of the supercell explanations.

perimental band gap, thus the conduction-band energies cannot be trusted. However, the impurity states of ZnS:Te consist of the valence bands. We did a projection analysis of the impurity state on to the bulk ZnS band states at all the k points and bands. We found that more than 99% of the projection is in the valence bands. Since the LDA formalism describes the valence bands well, we expect that the impurity states can be described well by LDA without further corrections. Binding energies ε_b (defined as the difference between the single-particle impurity state energy and the bulk VBM energy) for different sizes of supercell are shown in Fig. 5. Here, the bulk VBM energy is aligned to the supercell eigenenergies according to Ref. 41. In the 64-atom cell, our binding energy ε_b is 0.142 eV, while for the 4096-atom cell, this binding energy is only about 0.028 eV. The large drop of ε_b from the 64-atom cell result is the most dramatic character in Fig. 5. This indicates that the 64-atom cell is not converged with respect to the binding energy. This unconvergence can partly be explained by a coupling between the neighboring impurity states. When interaction exist between the neighboring impurity states, they form a bonding state at the $\bar{\Gamma}$ point with a higher energy (larger binding energy) and an antibonding state at the $\bar{X}$ point. We have calculated the $\bar{X}$ point $\mathbf{k}=(\pi/2a,0,0)$ impurity state binding energy for the 64-atom cell. This binding energy is 54 meV smaller than the binding energy at the $\bar{\Gamma}$ point. This energy difference is in the same order as the energy drop shown in Fig. 5. Finally, notice that the converged binding energy of 28 meV is rather small, indicating weak localizations.

Analyzing wave function in k space. Besides being displayed in real space, the wave functions can also be analyzed in reciprocal space. If an eigenfunction ψ_i is available, it can be projected into Bloch functions $\{u_{n\mathbf{k}}(\mathbf{r})e^{\mathbf{ikr}}\}$ of band index n and allowed reciprocal vector $\mathbf{k}$ within the first Brillouin zone. After summing up band index n, one gets a projection function,

$$P_i(\mathbf{k})=\sum_{n=1}^{\infty}|\langle\psi_i(\mathbf{r})|\mathbf{u}_{\mathbf{nk}}(\mathbf{r})e^{\mathbf{ikr}}\rangle|^2. \quad (5)$$

Figure 6 shows $P_i(\mathbf{k})$ for CBM state calculated from 512, 1728 and 4096 atom supercells. Notice that there is a single dominant $\mathbf{k}$ point that contains more than 99% of the total

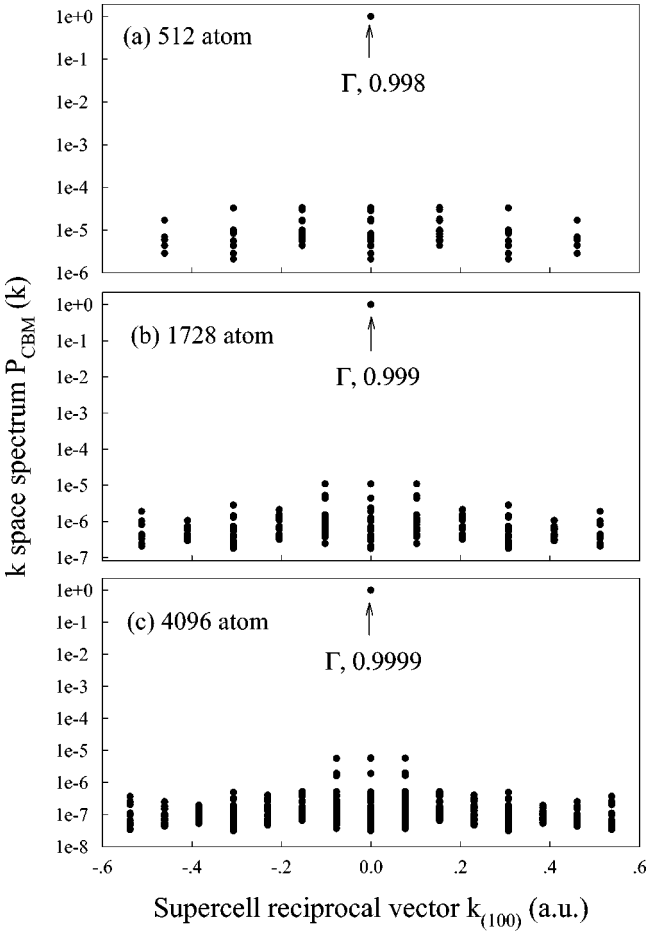

FIG. 6. k space spectrum $P_{CBM}(k)$ of the CBM state vs k point for (a) 512-atom supercell, (b) 1728-atom supercell, and (c) 4096-atom supercell.

spectral weight of $P_i(\mathbf{k})$. As shown in Fig. 6, when the size of the supercell increases the weight at Γ point is roughly a constant (actually it approaches 1 due to the fact that the center Te impurity atom has less and less effect on the CBM wave function). This dominant $\mathbf{k}$ point phenomena has been called "strong majority representation."[51] In the real space, $\psi_{CBM}(\mathbf{r})$ looks like a crystal Bloch state. Figure 7 shows the situation for the impurity states in ZnS:Te. The Γ point component $P_i(\Gamma)$ drops from 87% in the 512-atom cell to 58% in the 4096-atom cell. This is a typical manifestation of a real-space localized state. However, if we sum over $P_i(\mathbf{k})$ within a $2\pi/d_L$ box (dotted box in Fig. 7, where $d_L\sim 10$ Å is the rough localization size of the wave function according to Figs. 3 and 4), the result comes back to ~ 0.95. Thus, the width of the peak in reciprocal space is inversely proportional to the width of the localization in real space.

Transition intensities. The optical matrix element for direct transition coupling states (i) and (f) is given by

$$M_{if}=|\langle\psi_i|\mathbf{p}|\psi_f\rangle|^2. \quad (6)$$

The corresponding radiative emission rate and lifetime are calculated by

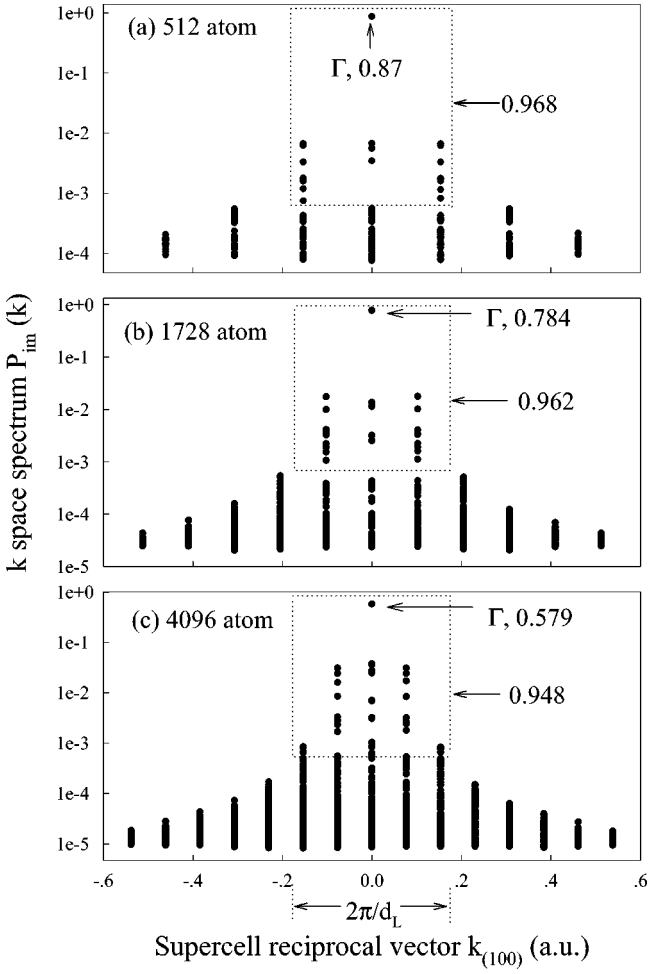

FIG. 7. Same as in Fig. 5, but for the impurity state in ZnS:Te. The dotted boxes sum over $P_{im}(k)$ within the a width of $\sim 2\pi/d_L$, where d_L is the localization size.

$$\frac{1}{\tau} = \frac{4\alpha\omega n}{3m_e^2c^2} M_{if}, \tag{7}$$

where α is the fine-structure constant, ω is the photon angular frequency, n is the refractive index (we use ZnS refractive index $n=2.3$ in this calculation). m_e is the free electronic mass, and c is velocity of light. The PL intensity is proportional to $M_{v,c}$ between the impurity state and the CBM states. The calculated $M_{v,c}$ for 64-, 512-, 1728-, and 4096-atom supercells including one Te impurity are 0.198, 0.183, 0.178, and 0.127 Ry, respectively. These can be compared with the bulk ZnS $M_{VBM,CBM}$ of 0.217 Ry. We see that although the impurity state is localized, a large matrix element still exists even for the largest supercell considered here. Note that $M_{v,c}$ decreases with the increasing supercell sizes. This change can be estimated by the change of $P_{im}(\mathbf{k}=\Gamma)$ shown in Fig. 7. Since the CBM's have essentially only the Γ point components as shown in Fig. 6, $M_{v,c}$ can be estimated as $P_{im}(\mathbf{k}=\Gamma)M_{VBM,CBM}$(bulk). Taking the values of $P_{im}(\mathbf{k}=\Gamma)$ from Fig. 7, we have the estimated $M_{v,c}$ as 0.189, 0.170, and 0.126 Ry for 512-,1728-, and 4096-atom supercells, respectively. This is in excellent agreement with the above directly calculated results. If we choose $M_{c,v}=0.127$ Ry, we obtain a lifetime $\tau=1.8$ ns. This corresponds well with the observed short recombination times (in the order of nanosecond) of localized excitons in ZnS:Te by time-resolved emission spectra.[26]

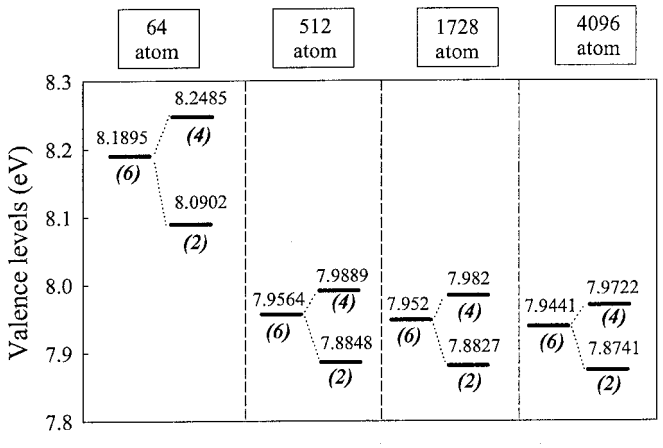

FIG. 8. Spin-orbit splitting of the impurity states calculated in different supercells. The left-hand bar indicates the level before the splitting. The numbers in the bracket indicate the degeneracy of the states.

Spin-orbit interaction. There is a strong spin-orbital coupling on the top of valence band for bulk ZnTe. Experimentally the spin-orbital splitting Δ_{SO} for ZnS is 68 meV, while $\Delta_{SO}=970$ meV for ZnTe.[48] One question is: how does the spin-orbit interaction alter the electronic structure for the impurity state. Using relativistic-effect-included nonlocal pseudopotentials and two-component spinor wave functions, we have first calculated the spin-orbital splitting for bulk ZnS and ZnTe. The results are 63.4 meV for ZnS, and 943 meV for ZnTe respectively, which are in good agreement with the above experimental values. We then use these relativistic-effect-included nonlocal pseudopotentials and spinor wave functions to calculate the impurity states for the various size supercells. The results are shown in Fig. 8. We see that the original sixfold (including spin) degenerated impurity states have been split into a fourfold degenerated state and a double-degenerated state, much like the Γ point situation in a bulk system. This spin-orbit splitting Δ_{SO} of the impurity state for 64-, 512-, 1728-, and 4096-atom supercells are 158, 104, 99, and 98, meV, respectively. They are much smaller than the ZnTe spin-orbit splitting, and slightly larger than the ZnS spin-orbit splitting. The converged spin-orbit splitting is about 98 meV. From the converged Δ_{SO} we can estimate the percentage of the impurity wave functions projected on the Te atom. Since the large Δ_{SO} of ZnTe is mostly due to Te atom for its strong core-level relativistic effect, given the percentage of the impurity wave function on Te as x, we have $\Delta_{SO}(\mathrm{ZnTe})x+\Delta_{SO}(\mathrm{ZnS})(1-x)=\Delta_{SO}(\mathrm{impurity})$. This gives us $x=4\%$. Thus, although it is the Te atom that causes the localized impurity state, there is only 4% of the impurity state wave function affected directly by the Te atom pseudopotential. Notice that the spin-orbit coupling also changes the impurity binding energy. For the top fourfold degenerated impurity state, the spin-orbit split-

ting up shifts their energy by $\frac{1}{3}\Delta_{SO}$(impurity)≈33 meV. But the VBM of bulk ZnS is also up shifted by $\frac{1}{3}\Delta_{SO}$(ZnS)≈23 meV. As a result, the impurity binding energy ε_b will be increased by 10 meV. Adding this to ε_b in Fig. 5, we get a final ε_b of about 0.04 eV.

C. Comparing the calculated binding energy to experiment

As we discussed in Sec. II C, we will use the constraint LDA approach to calculate the excited-state atomic relaxations and compare the results to experimental PLE, PL, and ZPL. In order to make a connection between our single-particle eigenenergy ε_b and the constraint LDA approach, we have calculated E_{LDA}(excited)$-E_{LDA}$(ground) for the 64-atom cell ZnS:Te. Here, E_{LDA}(excited) is the LDA selfconsistent total energy with one VBM unoccupied and one CBM occupied and with the same atomic configuration as in the ground state. We found this E_{LDA}(excited)$-E_{LDA}$(ground) is only 4 meV different from $E_g-\varepsilon_b$. This by itself is also a manifestation of the weak localization of the impurity state (for an infinitely large unlocalized state, it can be proved that the total energy difference equals exactly the single-particle eigenenergy).

For ZnS:Te there are experimental estimations of PLE caused by the impurity states, though the accuracy of these estimations is not as good as for PL. Note that, ZPL and PL can differ by a few tenths of eV. PLE should also be higher than ZPL. In previous calculations,[5,20] the calculated ε_b have been compared with the experimental PL. Given the big difference between PL, ZPL, and PLE, comparing to the correct spectroscopy peak is important. As shown above, our single-particle calculated $E_g-\varepsilon_b$ corresponds to the constraint LDA E_{LDA}(excited)$-E_{LDA}$(ground), and here the ''excited'' and the ''ground'' system have exactly the same atomic positions as in the ground state. Therefore, in a Franck-Condon picture[27,24] of Fig. 1, E_{LDA}(excited)$-E_{LDA}$(ground) should correspond to PLE. As a result , our calculated ε_b should be compared with experimental PLE, not with PL or ZPL. In Fig. 1 of Ref. 24, the intrinsic bulk exciton absorption peak E_{ex} is at 3.79 eV in ZnS with zinc-blend structure. The PLE spectrum E_s for single Te impurity is observed at 3.70 eV. Thus the impurity binding energy derived from PLE is around 90 meV. This is in fair agreement with our calculated ε_b of 40 meV given the uncertainties existed in the experimental results. Both the theory and experiment predict very shallow impurity states.

D. Atom relaxation and Stokes shift

LDA relaxation via VFF relaxation. In the above discussion the ground-state atomic positions are relaxed using total-energy LDA calculations for the 64-atom cell. We now test the accuracy of the VFF relaxation. Using the VFF relaxed atomic positions, we recalculated ε_b for the 64-atom cell. We find that this new ε_b differs by only 10 meV from the purely LDA relaxed results. We thus believe that the VFF relaxation for the ground state is adequate. We also tested the effect of fixing the ''surface atoms'' of the 64-atom cubic box in the charge patching method. To test that, we have relaxed all the atoms including the surface S atoms, and find that the results in ε_b differ by only 2 meV. In practice, the use of VFF atomic relaxation can save a lot of computational time. It takes more than 500 CPU hours to fully relax the atomic positions using the LDA method for a 64-atom system, while it only takes 80 CPU hours for a fixed atom LDA self-consistent calculation for the same system.

Small Stokes shift in LDA calculation. Stokes shift E_{Stokes} and Franck-Condon shifts $E_{FC1,2}$ are defined in Eq. (2) and Eqs. (3) and (4) respectively. We have calculated $E_{FC1,2}$ using 64-atom unit cells. In the one-dimensional configuration diagram of Fig. 1, one can find whether there will be a large Stokes shift from the minimum energy Zn-Te bond lengths of d_0 (for the ground state) and d_1 (for the excited state). If the difference between d_0 and d_1 is large, there is a large relaxation, and E_{FC1} and E_{FC2} are probably also large. Unfortunately, in the present calculation for one Te impurity, we found only small differences of the atomic relaxation between the ground state and the excited state. We find d_0 of 2.543 Å while d_1 is 2.564 Å. The corresponding Franck-Condon shifts for E_{FC1} and E_{FC2} are 10 meV and 8 meV, respectively, and the total Stokes shift is 18 meV. This is much smaller than the experimentally observed Stokes shift of ~560 meV.[24]

Our result of the small Stokes shift is consistent with previous LDA calculations for N impurity in ZnSe (Ref. 45) and As and P impurities in GaN,[19] all showing much smaller LDA calculated Stokes shifts than the experimental ones. At this stage, it is not clear what is the problem. One possibility is the 64-atom cell we are using. It might be possible that the long-range elastic relaxation, rather than the local atomic relaxation around the impurity atom is responsible for the large Stokes shift. Unfortunately, we cannot do total-energy calculation and atomic relaxations for systems much larger than 64-atom unit cells. Another possibility is the use of the constraint LDA method to describe the excited state. Due to the LDA band-gap error, the constraint LDA approach might be also in error. A more reliable way is to use *GW* plus Bethe-Salpeter equation to describe the exciton. Obviously, that is beyond the present day computer capability. Also note that all the current calculations for the Stokes shifts are carried out using pseudopotentials, it will be interesting to see the all-electron results.

Jahn-Teller effect. Now we will discuss the JT effect on ZnS:Te. A schematic model for trigonal JT distortion is shown in Fig. 2(b). Due to the difference between d_1 and d_2, the T_d symmetry has been lowered down to C_{3v} symmetry. This leads to a splitting of the sixfold degenerated t_2^6 impurity level into e^4 and a_1^2 levels. It is possible to lower the total energy under the C_{3v} JT distortion for the excited state using the constraint LDA approach. We found that the minimum energy for the excited state lies at a point with d_1 different from d_2 by 0.7% ($d_1=2.557$ Å and $d_2=2.540$ Å). This lowers the total energy by 48 meV compared to the minimum energy under T_d symmetry. This also leads to a e^4 and a_1^2 state splitting Δ_{JT} of ~20 meV. Even though we do find a Jahn-Teller splitting, this effect is too small to be used to explain the large Stokes shift. Actually,

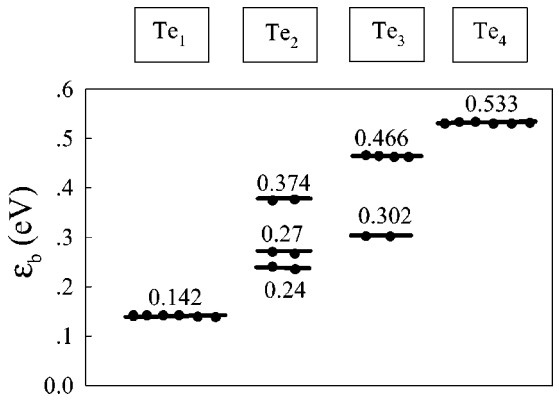

FIG. 9. The binding energies for Te_n $(n=1,2,3,4)$ clusters in ZnS. The spin-orbit interactions are not included in this calculation.

the Jahn-Teller effect we found is in the same order as the calculated Stokes shift under T_d symmetry.

The role of atomic relaxation in the binding energy of the impurity state. The atom relaxation is one of the main factors that affects the binding of the impurity state. Phillips[16] pointed out that the lattice deformations can weaken the binding energy of GaP:N, which was overestimated by Faulkner.[3] In our calculation, the binding energy for an unrelaxed (atoms are in the ideal zinc-blende positions) 64-atom ZnS:Te system is 0.064 eV, comparing to the binding energy of 0.142 eV for a relaxed system. Thus, in our case, the atomic relaxation helps the formation of a bound state, instead of weakening it. Our localized impurity state is caused probably more by the long-range strain field effect, than the chemical electronegativity effect.

E. Te_n clusters state

In a dilute ZnS:Te alloy, many experiments indicate the formation of Te_n clusters and their corresponding localized electronic states. We have calculated the electronic structure of Te_n clusters for $n=2,3,4$ using a 64-atom cell without spin-orbit interaction. The n Te atoms in the Te_n cluster share a common Zn bonding atom. The atomic positions for the clusters are relaxed using the VFF model. Figure 9(a) shows the binding energies of ZnS:Te with one Te impurity and $Te_n(n=2,3,4)$ clusters. Notice that, irrespective of the value n, the number of bound impurity state inside the ZnS energy gap is always 6 (counting the spin). This is interesting since if the n Te atoms are far apart, there would be $6n$ bound impurity states. For the Te_2 cluster, the symmetry of this system is C_{2v}. Since its irreducible representations are all in dimension one, there is no degeneracy (except the spin) in its eigenenergy. As a result, the sixfold degenerated state in Te_1 has been split into three energy levels as shown in Fig. 9. For Te_3, the symmetry group is C_{3v}. It contains dimension 2 and dimension 1 representations. Correspondingly, the sixfold degenerated state in Te_1 has been split into one fourfold degenerated state and one twofold degenerated state, much like the situation in JT split states. In Te_4, the system regains the T_d symmetry as in Te_1, thus has a sixfold degenerated state again. The binding energies of Te_n $(n=2,3,4)$ clusters are considerably larger than that for single Te impurity. The isosurface plots for the impurity wave-function squares are shown in Fig. 10. We have to mention that the current cluster calculations are done only in 64-atom cells. Although their binding energies are larger than the single impurity states, which indicate stronger localizations, it is likely that the energies shown in Fig. 9 are not completely converged with respect to the supercell sizes.

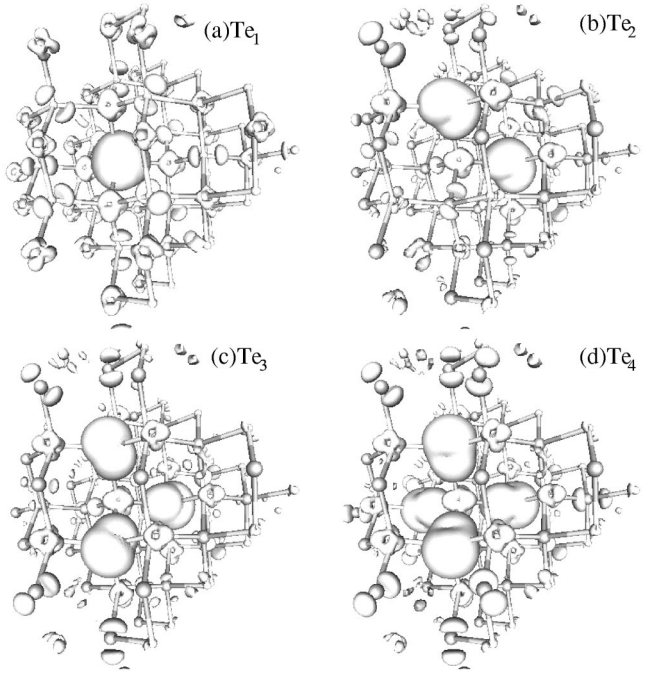

FIG. 10. The isosurface plots of the impurity state charge density for Te_n clusters: (a) Te_1, (b) Te_2, (c) Te_3, (d) Te_4. Note that Te_1 is just ZnS:Te, which has been shown in Fig. 3(a) in a cross-section plot. The charge densities of the three bound impurity levels (not counting spin) have been added up for these isosurface plots. The isosurface density value is 0.003 e/a.u. (Ref. 3) for all (a)–(d).

F. Impurity state pressure coefficient

In most isoelectronic impurities, the pressure dependence of the impurity level is similar to the host material. However, recently, Fang and Li found[31,32] that for a $ZnS_{1-x}Te_x$ $(x=0.005)$ sample, the pressure coefficient of a PL band (assumed to be coming from Te_1) is ~ 89 meV/GPa, much larger than that of bulk ZnS band gap (63.5 mev/GPa).[49] We have calculated the pressure coefficient of the impurity state energy $E_g-\varepsilon_b$. We have calculated this for the Te_1 impurity using a large supercell and Te_n clusters using the 64-atom supercell. The results are listed in Table IV in comparison

TABLE IV. The calculated and experimentally measured (Refs. 31,32) pressure coefficients of the photoluminescence energy related to Te_n clusters. The units are meV/GPa.

Te_n	Te_1	Te_2	Te_3	Te_4
Calculation	62.5	60.4	58.8	58.5
Experiment	89 ± 2	52 ± 3	59 ± 1	53 ± 1

with the experimental results. Notice that, our bulk LDA band-gap pressure coefficients for ZnS and ZnTe are 62.3 meV/GPa and 99.2 meV/GPa, which are close to the experimental results of 63.5 meV/GPa and 104 meV/GPa, respectively. For cluster Te_n with $n \geq 2$, the calculated results agree well with the experimental results, and all are close to the value of the host material ZnS. This is expected as we discussed before that the impurity states consist almost entirely of the host valence-band states. For the single Te impurity, our calculated pressure coefficient is still close to the host material, but the experimental results of Fang *et al.*[31,32] have a pressure coefficient of 89 meV/GPa. This could be just an anomaly of the single sample measured in Ref. 32. However, another possible reason could be that we have calculated the pressure coefficient of $E_g - \varepsilon_b$. As discussed before, this should be compared with the PLE peak, not with the PL peak. The pressure coefficient in Ref. 32 is for the PL peak. Thus, we need to calculate the Stokes shift, and calculate the pressure coefficient from that. Unfortunately, our calculated Stokes shift is small, and its pressure coefficient is also small. In practice, we found that the calculated pressure coefficient for $E_g - \varepsilon_b$ and for E_{PL} of Fig. 1(a) is almost the same. However, this could be a consequence of the failure of the LDA method to reproduce the large Stokes shift in the experiment. Further experiments and theoretical calculations are needed to clarify this point.

IV. CONCLUSION

In this paper we presented large scale LDA calculations for Te isoelectronic impurities in ZnS. The largest supercell we calculated contains 4096 atoms. This was possible due to the newly developed charge patching method. Regarding the questions we raised at the end of Sec. I, we have the following conclusions.

(1) Our LDA calculation indeed yields a bound state for ZnS:Te with t_2 symmetry and slightly above the top of valence band. The calculated binding energy is rather small about 40 meV, but it compares well with the experimental PLE data.

(2) Our converged impurity state is only weakly localized with only 16% of its wave function inside the 64-atom cell. Thus, the 64-atom cell calculation is severely unconverged, which yields a too large binding energy due to impurity-impurity interactions.

(3) The calculated impurity single energy level should be compared with the experimental PLE spectra, not with the PL or ZPL. Our calculated binding energy and the experimental PLE level both indicate a shallow impurity state.

(4) Using the Franck-Condon picture, our constraint LDA method yields a rather small Stokes shift of about 20 meV, an order of magnitude smaller than the experimentally observed Stokes shift of ~ 560 meV. However, this is consistent with previous LDA calculations for similar systems.[19,45] There are two possible reasons for the small Stokes shift in the calculation. The first one is the 64-atom cell we use in the excited-state atomic relaxation. This could be too small. The main effect of the atomic relaxation in the excited state might come from the long-range elastic relaxation, rather than the local relaxation near the impurity. The second possibility is the use of the constraint LDA method to describe the excited state. Notice that the large Stokes shift only exists in valence-band-induced isoelectronic states, not in the conduction-band-induced isoelectronic states. It would be very interesting to understand why. Further work is needed to clarify this point.

(5) Similar to the small Stokes shift, we found small Jahn-Teller distortion in the excited state, which splits the original t_2 state by 20 meV.

(6) We have also calculated Te_n clusters. With increasing n, their impurity state binding energies increase. But interestingly, for all $1 \leq n \leq 4$, there are always six (counting spin) bound states inside the band gap of host ZnS. For Te_1 and Te_4, the systems have t_2 symmetry and the states are sixfold degenerated. For Te_2 and Te_3, the systems have C_{2v} and C_{3v} symmetries, respectively. As a result their impurity states are split. We have also calculated the pressure coefficient of the impurity states. Our calculated pressure coefficients for Te_n are all close to bulk pressure coefficients of ZnS. This is consistent with the fact that all the impurity states consist almost entirely of the ZnS bulk valence bands. Our calculated pressure coefficient compare well with the experimental data for $n \geq 2$. But for Te_1, we did not reproduce the abnormally large pressure coefficient reported in Ref. 32.

(7) The spin-orbit interaction splits the six fold degenerated states in ZnS:Te into a fourfold degenerated states and a double degenerated states. The splitting is 98 meV, which is much smaller than the spin-orbit splitting for bulk ZnTe. From this, one can deduce that the impurity state wavefunction projection on the Te atom is about 4%.

ACKNOWLEDGMENTS

This work was supported by the Director, Office of Science, Basic Energy Science Division of U.S. Department of Energy under Contract No. DE-AC03-76SF00098. This research used the resources of the National Energy Research Scientific Computing Center, which is supported by the Office of Science of the U.S. Department of Energy. J. Li thanks Professor G. H. Li for providing experimental data of pressure coefficient for the Te_n cluster.

[1] D.G. Thomas, J.J. Hopfield, and C.J. Frosch, Phys. Rev. Lett. **15**, 857 (1965).

[2] D.G. Thomas and J.J. Hopfield, Phys. Rev. **150**, 680 (1966).

[3] R.A. Faulkner, Phys. Rev. **175**, 991 (1968).

[4] S.H. Sohn and Y. Hamakawa, Phys. Rev. B **46**, 9452 (1992).

[5] L. Bellaiche, S.H. Wei, and A. Zunger, Phys. Rev. B **54**, 17 568 (1996).

[6] W.M. Jadwisienczak and H.J. Lozykowski, in *Nitride Semicon-*

ductors, edited by F.A. Ponce *et al.*, Mater. Res. Soc. Symp. Proc. 482 (Materials Research Society, Pittsburgh, 1998), p. 1033.
[7] L.J. Guido, P. Mitev, M. Gherasimova, and B. Gaffey, Appl. Phys. Lett. **72**, 2005 (1998).
[8] Y. Zhang, A. Mascarenhas, H.P. Xin, and C.W. Tu, Phys. Rev. B **61**, 4433 (2000).
[9] W. Walukiewicz, W. Shan, K.M. Yu, J.W. Ager III, E.E. Haller, I. Miotkowski, M.J. Seong, H. Alawadhi, and A.K. Ramdas, Phys. Rev. Lett. **85**, 1552 (2000).
[10] A. Rubio and M. Cohen, Phys. Rev. B **51**, 4343 (1995).
[11] T. Mattila, S.H. Wei, and A. Zunger, Phys. Rev. B **60**, 11 245 (1999).
[12] L. Bellaiche, T. Mattila, L.W. Wang, and A. Zunger, Appl. Phys. Lett. **74**, 1842 (1999).
[13] J. Li and L.W. Wang, Phys. Rev. B **67**, 033102 (2003).
[14] J.J. Hopfield, D.G. Thomas, and R.T. Lynch, Phys. Rev. Lett. **17**, 312 (1966).
[15] W.G. Allen, J. Phys. C **1**, 1136 (1968); **4**, 1936 (1971).
[16] J.C. Phillips, Phys. Rev. Lett. **22**, 285 (1969).
[17] An-Ban Chen and B. Segall, Phys. Rev. B **12**, 600 (1975).
[18] An-Ban Chen and A. Sher, Phys. Rev. B **22**, 3886 (1980).
[19] T. Mattila and A. Zunger, Phys. Rev. B **58**, 1367 (1998).
[20] S.H. Wei, S.B. Zhang, and A. Zunger, J. Appl. Phys. **87**, 1304 (2000).
[21] I.K. Sou, K.S. Wong, Z.Y. Yang, H. Wang, and G.K.L. Wong, Appl. Phys. Lett. **66**, 1915 (1995).
[22] W.K. Ge, S.B. Lam, I.K. Sou, J. Wang, Y. Wang, G.H. Li, H.X. Han, and Z.P. Wang, Phys. Rev. B **55**, 10 035 (1997).
[23] J.D. Cuthbert and D.G. Thomas, J. Appl. Phys. **39**, 1573 (1968).
[24] T. Fukushima and S. Shionoya, Jpn. J. Appl. Phys. **12**, 549 (1973).
[25] S. Permogorov, A. Reznitsky, A. Naumov, H. Stolz, and W. van der Osten, J. Phys.: Condens. Matter **1**, 5125 (1989).
[26] A. Reznitsky, S. Permogorov, S. Verbin, A. Naumov, Yu. Korostelin, V. Korostelin, and S. Prokov'ev, Solid State Commun. **52**, 13 (1984).
[27] D.M. Roessler, J. Appl. Phys. **47**, 5387 (1976).
[28] O. Goede, W. Heimbrodt, and R. Muller, Phys. Status Solidi B **105**, 543 (1981).
[29] O. Goede, W. Heimbrodt, T. Lau, G. Matzkeit, and B. Selle, Phys. Status Solidi B **94**, 259 (1986).
[30] N.Z. Liu, G.H. Li, W. Zhang, Z.M. Zhu, H.X. Han, Z.P. Wang, W.K. Ge, and I.K. Sou, Phys. Status Solidi B **211**, 163 (1999).
[31] Z.L. Fang, G.H. Li, N.Z. Liu, Z.M. Zhu, H.X. Han, K. Ding, W.K. Ge, and I.K. Sou, Phys. Rev. B **66**, 085203 (2002).
[32] Z.L. Fang, F.H. Su, B.S. Ma, K. Ding, H.X. Han, G.H. Li, I.K. Sou, and W.K. Ge, Appl. Phys. Lett. **81**, 3170 (2002).
[33] P.R.C. Kent and A. Zunger, Phys. Rev. B **64**, 115208 (2001).
[34] J. Perdew and A. Zunger, Phys. Rev. B **23**, 5048 (1981).
[35] S.G. Louie, S. Froyen, and M.L. Cohen, Phys. Rev. B **26**, 1738 (1982).
[36] See website: http://www.nersc.gov/~linwang/PEtot/PEtot. html
[37] S.H. Wei and A. Zunger, Appl. Phys. Lett. **72**, 2011 (1998).
[38] C. Pryor, J. Kim, L.W. Wang, A.J. Williamson, and A. Zunger, J. Appl. Phys. **83**, 2548 (1998).
[39] L.W. Wang, Appl. Phys. Lett. **78**, 1565 (2001).
[40] L.W. Wang and A. Zunger, J. Chem. Phys. **100**, 2394 (1994).
[41] In a given supercell calculation, in order to align supercell eigenenergies with the bulk ε_{VBM}, we have aligned potential $V(r)$ at the corner of the supercell with the corresponding part in the bulk system.
[42] M. Li, D.J. Strachan, T.M. Ritter, M. Tamargo, and B.A. Weinstein, Phys. Rev. B **50**, 4385 (1994).
[43] T.M. Ritter, B.A. Weinstein, R.M. Park, and M.C. Tamargo, Phys. Rev. Lett. **76**, 964 (1996).
[44] V. Iota and B.A. Weinstein, Phys. Rev. Lett. **81**, 4955 (1998).
[45] S. Poykko, M.J. Puska, and R.M. Nieminen, Phys. Rev. B **57**, 12 174 (1998).
[46] J.L. Martins, N. Troullier, and S.H. Wei, Phys. Rev. B **43**, 2213 (1991).
[47] J.E. Bernard and A. Zunger, Phys. Rev. B **36**, 3199 (1987).
[48] *Numerical Data and Functional Relationships in Science and Technology*, edited by O. Madelung, M. Schultz, and H. Weiss, Landolt-Börnstein, New Series, Group III, Vol. 17, Pt. b (Springer, Berlin, 1982).
[49] S. Ves, U. Schwarz, N.E. Christensen, K. Syassen, and M. Cardona, Phys. Rev. B **42**, 9113 (1990).
[50] M. Cardona and D.L. Greenaway, Phys. Rev. **131**, 98 (1963).
[51] L.W. Wang, L. Bellaiche, S.H. Wei, and A. Zunger, Phys. Rev. Lett. **80**, 4725 (1998).